Pergamon

Journal of Structural Geology, Vol. 17, No. 6, pp. 875 to 886, 1995

0191-8141/95 $9.50 + 0.00

0191-8141(94)00103-0

Localization of duplex thrust-ramps by buckling: analog and numerical modelling

SHUMIN LIU* and JOHN M. DIXON

Experimental Tectonics Laboratory, Department of Geological Sciences, Queen's University, Kingston, Ontario, Canada, K7L 3N6

(*Received* 24 *March* 1992; *accepted in revised form* 22 *September* 1994)

Abstract—Duplex structures in natural fold-thrust belts occur over a wide range of geometric scales. Duplex thrust ramps exhibit a regular spacing linearly related to the thickness of strata involved in the duplex. We suggest that buckling instability in layered systems can produce local stress concentrations which localize thrust ramps with regular spacing. This mechanism is demonstrated through analog (centrifuge) and numerical (finite-element) modelling.

Centrifuge models containing finely-laminated multilayers composed of plasticine and silicone putty (simulating rocks such as limestone and shale) are compressed from one edge; folds propagate from hinterland to foreland. As shortening continues, the lowest competent unit is thrust into a blind duplex structure by break-thrusting. The duplex develops by serial nucleation of faults from hinterland to foreland; the ramp locations are inherited from the initial buckling instability.

Finite-element models based on the analog models and their natural prototypes demonstrate that stress concentrations develop in fore-limbs of anticlines within competent stratigraphic units. Models containing thrust discontinuities (at sites of calculated stress concentration) display additional stress concentrations in the fore-limbs of unfaulted folds closer to the foreland. The locus of stress concentration thus propagates towards the foreland, consistent with foreland thrust propagation in nature. The location and regular spacing of ramps are inherited from early (possibly even incipient) buckle folds.

INTRODUCTION

It has been well documented in many geological examples that thrusts in horizontal strata occur in imbricate arrays and generally follow flat–ramp–flat trajectories upward from a basal décollement towards the Earth's surface (e.g. Dahlstrom 1969, 1970, and many others). Mandl & Shippam (1981), Wiltschko & Eastman (1983, 1988), Bombalakis (1986, 1989), Schedl & Wiltschko (1987), Eisenstadt & De Paor (1987), Cello & Nur (1988), Platt (1988), Goff *et al.* (1990) and Goff & Wiltschko (1992), among others, have proposed various dynamic models to explain why thrusts ramp up from the basal décollement and why large-scale imbricate thrusts that originate as frontal thrusts have regular spacing. These include the influence of stratigraphic irregularities, stress oscillation due to stick-slip faulting, and stress redistribution in the underlying strata due to loading by the transported thrust sheet or to tapering of the overlying thrust sheet toward the foreland. Although these models have aided understanding of the mechanics of thrust ramping, particularly the formation of frontal ramps, none of them can explain the regularity of ramp spacing that is observed over the wide size range of natural duplex structures.

In duplex structures, a floor thrust and a roof thrust are linked by fault branches which ramp across the bedding and which commonly exhibit a relatively constant spacing as measured along the bedding, perpendicular to the strike of the faults (see below). Buckling instability is a characteristic of mechanically layered systems of all scales. A genetic connection between buckling and thrusting has been proposed by Heim (1878), Willis (1893), Currie *et al.* (1962), Dahlstrom (1970) and others. In an ongoing program of analog modelling of thrusting using the centrifuge technique, we have demonstrated that low-amplitude buckling of competent units may help to localize and hence control the spacing of thrust ramps in duplex structures (Dixon & Tirrul 1991, Liu 1990, Liu & Dixon 1990, 1991, Dixon & Liu 1991). Morley (1994) has applied the concept and our model results to a particularly well-documented natural example in the Caledonides. In the present paper, we extend our examination of this hypothesis by combining the results from analog (centrifuge) and numerical (finite-element) modelling.

SPACING OF THRUST RAMPS IN DUPLEXES

In this section we document a consistent relationship between thrust-ramp spacing and thickness of duplexed stratigraphic interval, and draw a parallel with the wavelength-thickness relationship for buckling.

A striking feature of well-constrained structural cross-section through fold-thrust belts is the apparent regularity of spacing of thrust ramps in duplex structures of many sizes. We have measured the spacing of ramps or imbricates from restored cross-sections of 16 duplex structures from different thrust belts including the Valley and Ridge Province of the Appalachian Moun-

*Present address: Husky Oil Operations Ltd., 708 8th Avenue SW, P.O. Box 6525, Station D, Calgary, Alberta, Canada, T2P 3G7.

Table 1. Thrust spacing and duplex height

Natural Duplex Structures Orogenic belt (source, Fig., section)	Duplex height* (m)	Number of horses	Average spacing† (m)	Standard deviation (m)	Normalized standard deviation‡
Appalachians, U.S.A (Woodward 1985, section 6)	2860	7	15,540	2390	0.15
Appalachians, U.S.A. (Evans 1989, Fig. 10, section C–C′)	3430	16	9120	3700	0.4
Brooks Range, Alaska, U.S.A. (Mitra & Namson 1989, Fig. 4, section B)	2500	5	11,120	2600	0.23
Canadian Rocky Mountains (Fermor & Price 1987, Figs. 10 and 11)	94 110	19 5	144 274	82 89	0.57 0.32
Canadian Rocky Mountains (Price 1981, Fig. 2, section SW–NE)	1930	5	4920	360	0.07
Canadian Rocky Mountains (McMechan 1985, Fig. 4)	1524	3	16,130	880	0.05
Canadian Rocky Mountains (Skuce *et al.* 1992, Fig. 2, duplex 'A')	250	3	800	0.0	0.0
Sawtooth Range, Wyoming, U.S.A. (Mitra 1986, Fig. 24)	4	3	11.9	0.5	0.04
Wasatch Range, Utah, U.S.A. (Schirmer 1988, Fig. 6, section C–C′)	330	3	2520	730	0.29
Alps, Switzerland (Boyer & Elliott 1982, Fig. 32)	2270	3	8790	725	0.08
Moine Thrust Belt, Scotland (Elliott & Johnson 1980, Fig. 18, sections M–M′ and K–K′)	95 27	6 4	555 735	145 340	0.26 0.46
Scandinavian Caledonides (Townsend *et al.* 1986, Fig. 3)	340	12	1590	800	0.5
Himalaya, Pakistan (Banks & Warburton 1986, Fig. 5)	7060	7	31,770	6160	0.19
Papuan Fold Belt, New Guinea (Hill 1991, Fig. 5)	2230	4	10,830	1490	0.14
Analog-Model Duplex Structures Source (model number)	Duplex height* (mm)	Number of horses	Average spacing† (mm)	Standard deviation (mm)	Normalized standard deviation‡
Liu & Dixon (1990) (Model TH-24)	1.0	9	6.11	2.11	0.35
Liu (1990) (Model TH-15)	1.33	7	7.92	3.13	0.39

*Stratigraphic interval between roof thrust and floor thrust.
†Bed length between adjacent thrust ramps, measured in transport direction.
‡(Standard deviation) ÷ (average spacing).

tains (U.S.A.); the Rocky Mountains (Canada and U.S.A.); the Himalaya; the Caledonides (Norway); and the Moine Thrust belt (Scotland). For each duplex, we measured the duplex height (the thickness of strata between the roof thrust and floor thrust) and calculated the average spacing (bed length measured across strike) of thrust ramps that bound a number of horses constituting the duplex structure. The data and their sources are listed in Table 1. For each duplex, the normalized standard deviation of average thrust spacing (standard deviation divided by average spacing) generally varies from zero to one third of the average spacing, though some extreme values exist. This suggests a strong tendency for duplex thrusts to have regular spacing.

Figure 1 shows empirically that there is a general linear relationship in log–log space between the spacing of thrusts and the stratigraphic thickness of the duplexed interval. Admittedly, other variables such as rock rheology (influenced by mineralogy, grain size, water content, temperature, confining pressure) and rate of stress application might also be expected to play a role; indeed, such variables are likely responsible for much of the scatter in the data.

The measurements include several potentially significant sources of uncertainty. First, there is considerable variation among the stratigraphic successions included in the duplexes we measured. Thus, the measured heights include various unknown thicknesses of incompetent strata in addition to that of the main mechanical unit that dominates a duplex. Second, the stratigraphic units are likely to have been thickened by ductile strain associated with homogeneous layer-parallel shortening. Third, while fault spacing was measured parallel to bedding on restored cross-sections, the restoration pro-

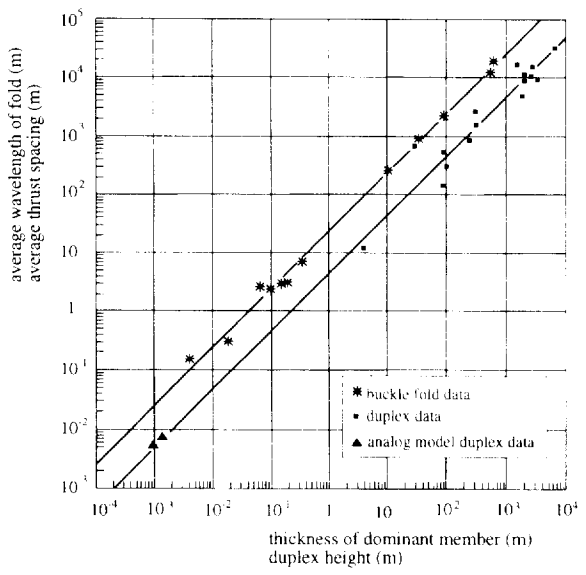

Fig. 1. Empirical relationships between stratigraphic thickness and structural 'wavelength' (log–log plot). Solid squares show the relationship between average thrust spacing (measured from balanced cross-sections in the papers listed in Table 1) and duplex height (the stratigraphic thickness of rocks between roof and floor thrust, in restored state). Stars show the relationship between the wavelength of buckling and the thickness of 'dominant' stratigraphic units (mainly sandstones) within incompetent strata (mainly shales) from localities in the Appalachian Valley and Ridge province and the Rocky Mountains foothills (from Currie *et al.* 1962). Data for duplex thrusts and buckle folds are plotted on the same diagram for ease of comparison, but see text for a discussion of differences between the measured quantities. The straight lines were fitted to the two sets of data points by least-squares regression. The line through the duplex data has a correlation coefficient of 0.95, a residual standard deviation of 0.002, and a slope of 0.98 (44.5°). The line through the fold data has a correlation coefficient of 0.99, a residual standard deviation of 0.0003 and a slope of 0.97 (44°). The solid triangles indicate measurements of thrust spacing obtained from analog models TH-15 and TH-24 (Liu & Dixon 1990). Model points were not used in regression of the line through the duplex data.

cess may not have properly corrected for layer-parallel shortening [which has been estimated to account for 10–35% of the total shortening in some fold-thrust belts (e.g. Protzman & Mitra 1990, Holl & Anastasio 1993)]. The net result of these uncertainties is that the primary stratigraphic thickness of a duplex is likely to be overestimated and the primary spacing of thrust ramps is likely to be underestimated. Nevertheless, the regularity of thrust spacing in a duplex and its linear dependency on duplex height suggest that there is an internal mechanism which controls duplex thrust spacing.

This relationship between thrust spacing and duplex height is similar to that between fold wavelength and competent-member thickness documented by Currie *et al.* (1962; see Fig. 1), although for equivalent measured stratigraphic thickness, thrust spacing is greater than fold wavelength. However, direct comparison between the data sets is difficult because there is a fundamental difference between the two sets of thickness measurements. On the one hand, while recognizing that the wavelength of folds is influenced by interference among adjacent layers, Currie *et al.* (1962) measured only the thickness of a single 'dominant member' within each buckled stratigraphic interval. On the other hand, we have measured the total thickness of the stratigraphic interval between floor and roof thrusts of each duplex, an interval which may include the incompetent strata in addition to the principal competent duplexed unit, and may include more than one 'dominant member'. Thus the expected sense of discrepancy between the two data sets is that duplex thickness should be too large or fold thickness too small at a given 'wavelength', as observed (see Fig. 1).

To compare the two data sets would require detailed analysis of each stratigraphic section using modern buckling theory, an undertaking which was beyond the scope of the present study. This approach has been pursued by Goff *et al.* (1990) in reference to the spacing of major thrusts (formed as frontal ramps) in the Idaho–Wyoming thrust belt. They concluded that the spacing of major thrusts does not correspond to the theoretical buckling wavelength of the stratigraphic section. Goff & Wiltschko (1992) then investigated other dynamic controls on the spacing of frontal ramps. We stress that the present investigation focuses just on duplex thrusts.

While the measured data do not demonstrate coincidence between buckling wavelength and the spacing of duplex thrusts, the senses of the discrepancies between the two types of measurements suggest that buckling and duplex thrusting may have similar dependence on the thickness of the stratigraphic interval involved. An extension of this conclusion is that the two processes may be related; that is, thrust ramps may be localized by folding. (It should be noted that this mechanism should not be expected to yield identical spacing for folds and ramps, because not every fold is likely to become faulted; therefore the average spacing of thrusts should be greater than the wavelength of folds in a given stratigraphic interval. This tendency is also in the same sense as the discrepancy noted between the two data sets.)

Currie *et al.* (1962, p. 669) entertained the same hypothesis: "there is the possibility that thrusts develop as a result of advanced folding", and in so doing were following Heim's (1878) concept of 'stretch thrusts'. In the present paper we examine the validity of this causative relationship through analog and numerical modelling.

ANALOG MODELLING

Method and model configuration

Analog modelling using the centrifuge technique (Ramberg 1967, 1981) and appropriate model materials (Dixon & Summers 1985) can achieve considerable geometric and dynamic similarity between the models and the natural prototype system. It has the great advantage that the kinematic evolution of structures can be documented while a model is deformed in stages. We have applied the centrifuge technique in an analog modelling study of fold-thrust tectonics. The details of the technique, the initial geometry and kinematic evol-

Table 2. Model ratios applicable to model TH-24

Quantity	Ratio	Equivalence Model = prototype
Length	$l_r = 1.0 \times 10^{-6}$	10 mm = 10 km
Specific gravity	$\rho_r = 0.6$	1.60 = 2.67 (bulk value for whole stratigraphic column)
Acceleration	$a_r = 4.0 \times 10^{3}$	4000 g = 1 g
Time	$t_r = 1.0 \times 10^{-10}$	1 hour = 1.15 Ma (for example)
Stress	$\sigma_r = \rho_r l_r a_r = 2.4 \times 10^{-3}$	(calculated from other ratios)
Viscosity	$\mu_r = \sigma_r t_r = 2.4 \times 10^{-13}$	(calculated from other ratios)

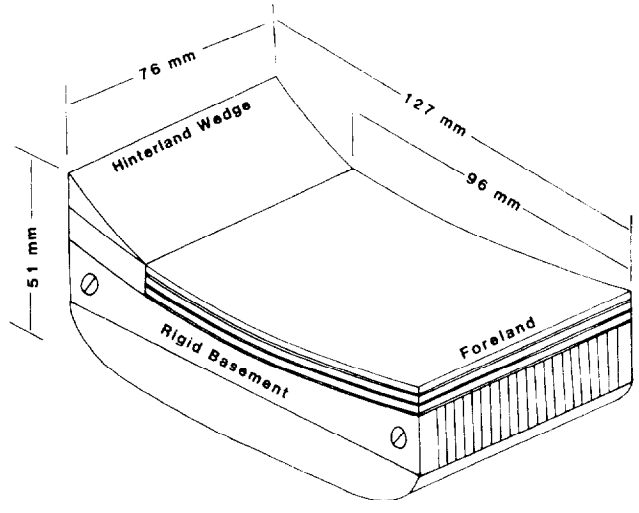

Fig. 2. Dimensions and initial configuration of analog model TH-24 (after Liu & Dixon 1990).

ution of the models, and their similarity to selected natural prototypes have been presented elsewhere (Dixon & Tirrul 1991, Liu & Dixon 1990, 1991, Dixon & Liu 1991). We will repeat here only a brief summary, to familiarize the reader with the process, and focus on one typical model (TH-24).

The model is constructed of laminae of Plasticine® and silicone putty, materials which are suitable mechanical analogs for limestone and shale, respectively, under conditions expected within a deforming fold-thrust belt and for the scale-model ratios chosen (Dixon & Summers 1985, Dixon & Tirrul 1991; see Table 2). The stratigraphic sequence contains six units of alternating bulk competency (high/low/high/low/high/low from top to bottom). The three competent units each contain four equal-thickness laminae of plasticine of different colours (black, red, blue and yellow) with a total thickness of 1.00 mm; the incompetent units each contain 4 laminae, two of silicone putty and two of black plasticine in a thickness ratio of 2:1 and with a total thickness of 0.33 mm. The thickness of the full stratigraphic pile is 4 mm. Figure 2 shows the initial configuration of the model.

Fold-thrust evolution

The model was subjected to horizontal compression from one end by gravitational collapse and lateral spreading of a plasticine wedge (Fig. 2). It was shortened in six stages, and sections cut between successive stages. The progressive evolution of the model (through stages I–VI) is shown in profile view (vertical sections parallel to the shortening axis) in Fig. 3.

In early stages, the structure is characterized by buckle-fold trains in the three competent units, and localized, grouped small folds in incompetent units. After stage II, the buckle folds pervade the section, but their amplitudes decrease towards the foreland. During stage II, three thrusts developed in the fore-limbs of previously-formed low-amplitude folds in the lowest competent unit, their displacements decreasing from the hinterland towards the foreland.

During stage III, the folds in the upper and middle competent units continued to increase in amplitude, and new thrusts developed within the lowest competent unit, in folds situated on the foreland side of those thrusts formed at earlier stages. Earlier-formed thrusts continued to increase their displacement even as new thrusts nucleate. This evolution is documented in detail in Liu & Dixon (1990) and Dixon & Liu (1991), and this kind of evolution was also reported in the Rocky Mountain fold and thrust belt of North America by Boyer (1991) who characterized it as 'synchronized thrusting'.

An evolutionary relationship between folding and thrusting can be observed in the lowest competent unit of the model (Figs. 3 and 4; see detailed description in the caption of Fig. 3). The structures evolve as follows: a fold nucleates first and localizes a thrust ramp in its foreland-dipping limb; the fold grows and tightens as the fault propagates through its front limb; the hanging-wall anticline's shape is further modified as it is transported through the upper fault bend. Folding and thrusting alternate in the dominant role during the deformation process, but folding occurs first and the thrust ramps are 'break-thrusts' as defined by Willis (1893). From this description (see also Liu & Dixon 1990, 1991, Dixon & Liu 1991), it is clear that the earlier-stage low-amplitude folds in the competent units play a major role in localizing the thrust ramps. The thrust ramps within the lowest competent unit have a regular spacing (see Table 1) which is inherited from the buckle-fold train. The striking similarity of the model structures to natural duplexes (Liu & Dixon 1990, 1991, Morley 1994) suggests that this mechanism also operates in nature.

The question remains: Why do the thrusts propagate upwards through the front limbs of the folds? It is

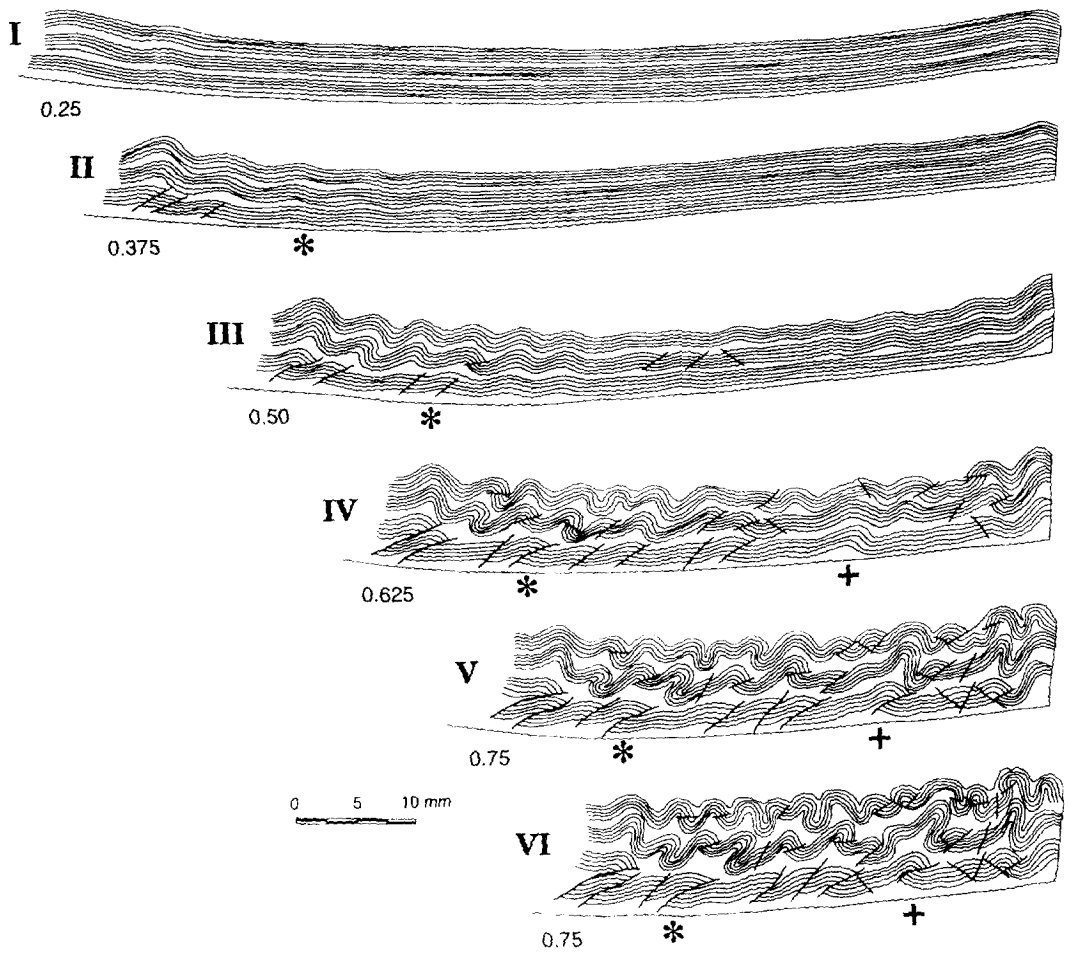

Fig. 3. Line-drawings of vertical sections through model TH-24 at stages I through VI (from Liu & Dixon 1990). Decimal values indicate the lateral positions (in inches) of the sections relative to one edge of the model. Structures in the lowest competent unit exhibit an evolutionary relationship between folding and thrusting. For example, at stage II the structure marked by the asterisk (*) is a low-amplitude 'detachment' fold (Jamison 1987) which overlies a zone of décollement in the basal incompetent unit. At stage III, the lower part of the lowest competent unit is displaced by a propagating thrust ramp and the fold has become a 'fault-propagation' fold (Suppe & Medwedeff 1984, Suppe 1985, Suppe & Medwedeff 1990) which grows in amplitude as the fault propagates. By stage IV, the thrust has propagated completely through the lowest competent unit and into décollement within the overlying incompetent unit. Now the fault has a flat–ramp–flat trajectory and the upper fault bend begins to influence the shape of the fold. In stages V and VI the fold evolves into a well-developed 'fault-bend' fold (Suppe 1983), although because of its complex history its geometry may not match that predicted for pure fault-bend folds. Other structures in the lowest competent unit, especially the one marked by the plus sign (+), also follow this evolution. See text and Fig. 4.

reasonable to suspect that foreland-dipping fold limbs may be sites of stress concentrations sufficiently intense to localize fault rupture. We test this hypothesis using finite-element modelling in the following section.

FINITE-ELEMENT ANALYSIS

Method

Finite-element analysis can determine stresses, displacements and strains in a body with specified rheology and boundary conditions (Reddy 1984, Burnett 1987). It has been widely applied to geological problems (e.g. Dieterich 1969, Dieterich & Carter 1969, Berner *et al.* 1972, De Bromaeker & Becker 1978, Müller & Briegel 1980, Schedl & Wiltschko 1987).

The purpose of using the finite-element method in the present study is to determine how the stress field varies locally within the horizontally-loaded foreland strata in order to identify possible stress concentrations which might localize the nucleation and control the propagation of faults. The finite-element models were designed to simulate the relevant geometric and mechanical properties and boundary conditions of prototypes that are also represented by analog models such as the one described above.

As this is a first-order test of the hypothesis that folds can induce stress concentrations that might localize thrust ramps, we have not performed an exhaustive parametric study involving numerous fold geometries and a range of fold amplitudes. Furthermore, we have not attempted to model the growth to finite-amplitude buckle folds. We use a linear elastic model because we seek only to determine the instantaneous stress distribution within strata that were previously buckled (albeit by viscoplastic flow). The elastic parameters used were

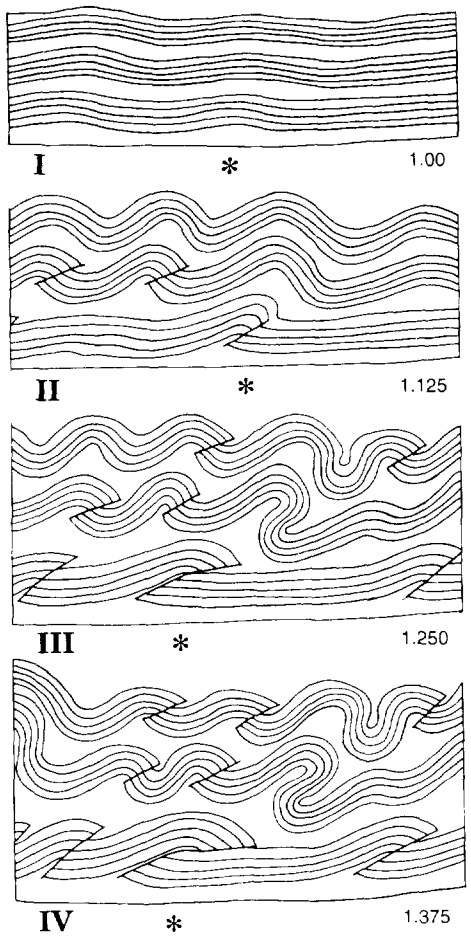

Fig. 4. Line-drawings (detail) of vertical sections through model TH-24 (Fig. 3) at stages II through V (from Dixon & Liu 1991). Decimal values indicate the lateral positions (in inches) of the sections relative to one edge of the model. The evolutionary relationship between folding and thrusting in the lowest competent unit is documented by the structure marked by the asterisk (*). See text and caption for Fig. 3.

obtained from tests on small intact samples, so the strength of the rock mass is exaggerated. However, as we are interested in orientation patterns and relative stress concentrations rather than absolute stress levels, this simplification seems justified. We emphasize that the stress levels calculated in the finite-element analyses should not be taken as representative of stress levels expected in the prototype system.

The modelling employed the program ABAQUS (Hibbitt, Karlsson and Soresen Inc.) on an IBM ES9000 main-frame computer at Queen's University. Accuracy was checked by testing convergence and by recalculation using models with element grids discretized at a smaller scale.

Configuration of the models

Three sets of models were designed on the basis of the centrifuge modelling. The numerical models represent prototypes measuring 96 km long and 4 km thick, scaled from the centrifuge models. All the numerical models contain six stratigraphic units, three competent units and three incompetent units. The three sets of numerical models differ in that the first (series H, Fig. 5a) contained horizontal strata; the second (series F, Fig. 5b) incorporated a train of three low-amplitude fold culminations on the left-hand (hinterland) side; and the third (series FT, Fig. 5c) incorporated not only fold trains but also thrust faults in the lowest competent unit. In series FT the incompetent units accommodate distributed deformation that represents floor and roof thrusts which are linked by duplex ramps that climb across the lowest competent unit. In all models the strong units were modelled with the elastic properties of limestone, and the weak units with those of shale (Touloukian *et al.* 1983, Carmichael 1982) (see Table 3).

In all the models the right-hand vertical boundary (the 'foreland' end) is fixed. This does not correctly simulate the buttressing effect of a semi-infinite sheet, and therefore the right-most end of the models should be neglected. The floor boundary is also fixed, with neither horizontal nor vertical movement of nodes permitted. This simulates a high-strength ('glued') contact between the stratigraphic pile and a rigid basement. A constant horizontal compressive stress (150 MPa) was applied to the left-hand ('hinterland') boundary. The nodes at this boundary may move vertically while the boundary is displaced to the right as a vertical plane. The top boundary (representing the Earth's free surface) is free to move in any direction. The calculation includes gravity and incorporates a plane-strain boundary condition.

The boundary conditions in the finite-element models can be compared with those in the analog models as follows: both have a fixed foreland boundary; the basal boundary in the analog models is able to slip laterally once its shear strength is exceeded, while that in the finite-element models is fixed; the hinterland interface of the stratigraphic pile is constrained to remain vertical in the finite-element model whereas it is free to deform and rotate in the analog models; and the top surface is unconstrained in both systems.

The fault surfaces in models of series FT are represented by one-dimensional interface elements. The mechanical behaviour of these surfaces is defined by the coefficient of friction of the classical Coulomb friction law: the shear strength of the interface element varies in proportion to the normal (compressive) stress acting across it; displacement cannot occur on the surface unless the shear stress reaches this frictional limit. The pre-existing faults are non-cohesive and have a coefficient of internal friction of 0.57.

A total of 13 calculations were performed with different applied stresses and different mesh sizes. The aim of using different numbers of elements was to check the accuracy of the analysis. The results from three calculations (models H2, F1 and FT1) are discussed here. The finite-element grids for these three models are shown in Fig. 5. The program (ABAQUS) computes output at four interpolated points within each four-node element, and at three points within each three-node element.

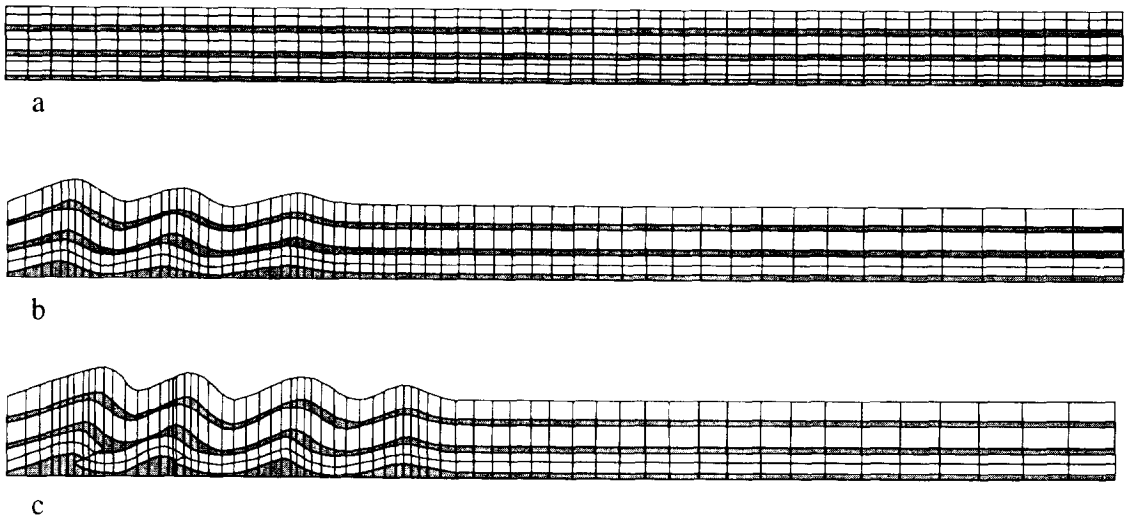

Fig. 5. The configuration and finite-element grids of (a) model H2 with only horizontal strata (500 four-node elements), (b) model F1 with built-in low-amplitude folds (441 four-node elements), and (c) model FT1 with both folds and thrusts (478 four-node elements, 12 three-node elements and 6 four-node interface elements). Stippled: incompetent units. Plain: competent units. Boundary conditions: lower and right-hand boundaries are fixed; left-hand boundary is free to move horizontally as a vertical plane; top surface is free.

Table 3. Material properties used in finite-element models

Material	Density (kg m^{-3})	Young's modulus (Pa)	Poisson's ratio (ν)
Limestone	2400	7.0×10^{10}	0.3
Shale	2400	3.5×10^{9}	0.2

(Touloukian *et al.* 1981, Carmichael 1982.)

Analytical results

Model with horizontal strata. We computed the stress distribution in horizontal strata as a baseline against which the influence of folds and faults can be compared.

The spatial variation of orientation of the maximum principal stress (σ_1) in model H2 is shown in Fig. 6(a). There is a gradient of σ_1 orientation in the three competent units, from horizontal at a high level at the hinterland end to steeply-plunging and vertical at depth and towards the central part of the model. At the foreland end (approximately the right-most 20% of the model) the effect of the rigid end boundary is seen as a disturbance of the regular gradient. There is a similar gradient within the weak units, although σ_1 everywhere has a steeper plunge than in the stiff units. This pattern is like that of Hafner (1951). It differs in that the trajectories deflect across the material boundaries (whereas Hafner's calculation dealt with a homogeneous block). See also Treagus (1981, 1983) for a theoretical treatment of stress/strain refraction across boundaries between layers of contrasting viscosity. The trajectories are much steeper in model H2 than in Hafner's calculation, especially in the centre part of the model where they become nearly vertical, because of the influence of gravity forces. In this area, the load applied at the hinterland end of the model has little influence and the stress is largely induced by gravity. This is compatible with *in situ* stress measurements [see, e.g. data summarized by Suppe (1985)] indicating that the vertical stress is greater than the horizontal stress in regions where the stress field is induced mainly by gravity.

The spatial variation of the values of maximum principal stress (σ_1) and differential stress ($\sigma_1 - \sigma_3$) is shown by the contours in Figs. 6(b) & (c), respectively. The stress values are highest at the hinterland end of the model, within the stiff layers, and decrease monotonically towards the foreland. In the central part of the model, where the effect of the end-load is not significant, the stress contour lines are parallel to the material boundaries and the value increases with depth due to gravity. The lowest values of σ_1 and differential stress ($\sigma_1 - \sigma_3$) occur in the central part of the uppermost strong unit. The moderate stress concentration at the foreland end of the model is due to the fixed boundary condition and should be ignored.

This model exhibits an overall stress concentration (in the stiff layers) within a triangular region in front of the loaded hinterland boundary. Failure would be anticipated to initiate in the vicinity of the top left end. Although modified here by the presence of layers with contrasting strength, the overall pattern of stress is consistent with Coulomb wedge theory (Davis *et al.* 1983). As failure initiates, the stratigraphic pile would be thickened at the hinterland end and the stress concentration would expand to the right, towards the foreland. However, the monotonic stress gradient does not provide a basis of expecting failure to nucleate at any particular point distant from the hinterland boundary.

The variation of orientation of the principal stress axes in the hinterland portion of model H2 (σ_1 shown in Fig. 6a) is compatible with development of foreland-verging thrust faults that are listric and have a stair-step (flat–ramp–flat) trajectory through the stratigraphic pile. Surfaces of shear failure should have low dips within the weak units and steeper dips within the stiff units, and their dips should steepen from the lowest to the topmost stiff unit.

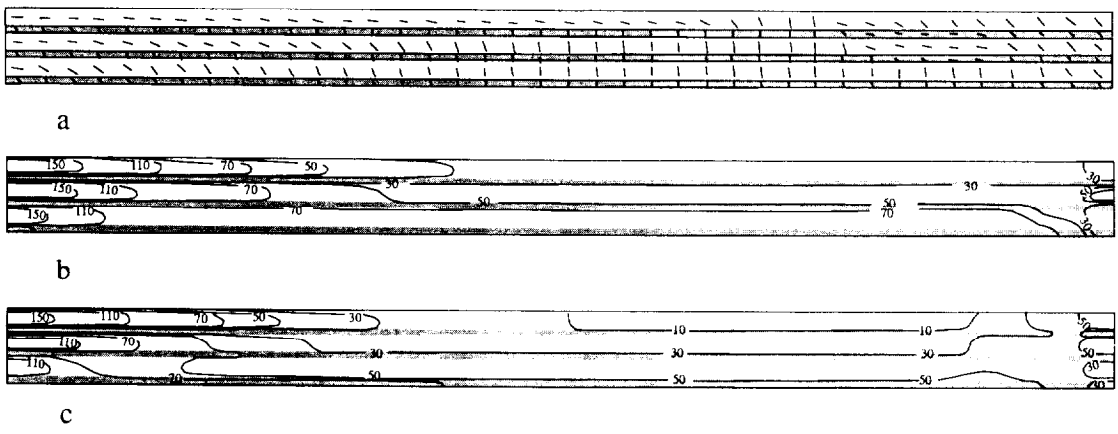

Fig. 6. Finite-element analysis results for model H2. Boundary conditions as in Fig. 5. Horizontal compression is applied to the left-hand boundary. (a) Orientations of maximum principal stress (σ_1). (b) Contour map showing the spatial variation of maximum principal stress (σ_1), MPa. (c) Contour map showing the spatial variation of differential stress ($\sigma_1 - \sigma_3$), MPa.

Model with low-amplitude folds. The models of series F (Fig. 5b) were designed such that their geometry was similar to that of the analog models after the early stages of deformation, when low-amplitude folds had formed in the rear part of the model foreland (e.g. model TH-24, stages I and II; see Fig. 3). The aim of the calculations on series F is to determine the stress distribution in such folded layering for comparison with that in models with horizontal strata.

The spatial variation of orientation of the maximum principal stress (σ_1) in model F1 is shown in Fig. 7(a). The general pattern is similar in many respects to that of model H2 (Fig. 6a): σ_1 is steeper in weak units, while its plunge in stiff units steepens with depth and distance from the loaded boundary. However, the folds have a strong influence on the attitude of σ_1 in the stiff units. σ_1 plunges diagonally across the bedding in the back (hinterland-dipping) limbs of the anticlines but tends towards parallelism with bedding in the front (foreland-dipping) limbs.

The stress orientations in the folds in this model differ systematically from those calculated by Dieterich & Carter (1969) for buckled viscous multilayers. In their model, σ_1 consistently plunged in the same direction as the dip of the fold limbs, whereas in this model it plunges towards the foreland. There are several reasons for this difference. There was stronger stress 'channelling' in Dieterich & Carter's (1969) model because it had a single thin strong layer embedded in a thick weak matrix, whereas here the weak units are thinner so there is more coupling between the several stiff layers. Dieterich & Carter's models were symmetrical because the compression was applied at both ends and the top and bottom surfaces were beyond the zone of influence of the folding; here, in contrast, the load is applied at one end only, and the top surface is free and the bottom fixed. Finally, their analysis did not include gravitational forces because they were studying small-scale folding. All of these factors contribute to rotate σ_1 into a foreland-plunging attitude in our finite-element model F1.

We have also computed the orientations ($\pm 45°$ to σ_1) of the planes of maximum shear stress (τ_{max}) in model F1. Figure 7(b) shows the two orthogonal orientations for each element. For most rocks, with a coefficient of internal friction in the range 0.5–1.0 (Jaeger & Cook 1979), Coulomb shear failure of intact material would occur on planes inclined at $\pm 22°$–$32°$, rather than at $\pm 45°$, to σ_1. Nevertheless, this plot conveys an approximation of the expected orientations of potential shear failure. In the foreland-dipping limbs of folds in the stiff units, one of the two conjugate planes of τ_{max} is inclined to the layer in an orientation compatible with formation of foreland-verging thrust faults that would ramp across the bedding as 'break-thrusts'. In the hinterland-dipping limbs, one τ_{max} plane is at a lower angle or even parallel to the layering and is less-favourably oriented for the formation of thrust ramps. This is also consistent with the observation that back-thrusts, if they develop, have higher angles relative to bedding (and steeper dips) than do fore-thrusts (Chapple 1978, Tirrul 1983, Davis *et al.* 1983).

The spatial variation of the values of maximum principal stress (σ_1) and differential stress ($\sigma_1 - \sigma_3$) in model F1 is shown by the contours in Figs. 7(c) & (d), respectively. For the sake of clarity, the left-hand (hinterland) portions of these plots are reproduced at enlarged scale in Figs. 7(e) & (f). Both patterns differ substantially from those of the plane-layered model H2 (Figs. 6b & c). While the stress levels are still generally higher at the hinterland end, there is no longer a smooth monotonic gradient from left to right; rather, there are distinct localized concentrations of stress within the stiff layers, in the foreland-dipping limbs of the folds. This is most marked in the lowest stiff layer where σ_1 exceeds 300 MPa and 200 MPa in the left-hand and middle folds, respectively. The right-hand fold in the lowest stiff layer also exhibits a small but significant concentration (100 MPa) relative to the immediate surroundings. The differential stress pattern exhibits similar, and indeed even more pronounced, concentrations that are clearly localized in the foreland-dipping fold limbs.

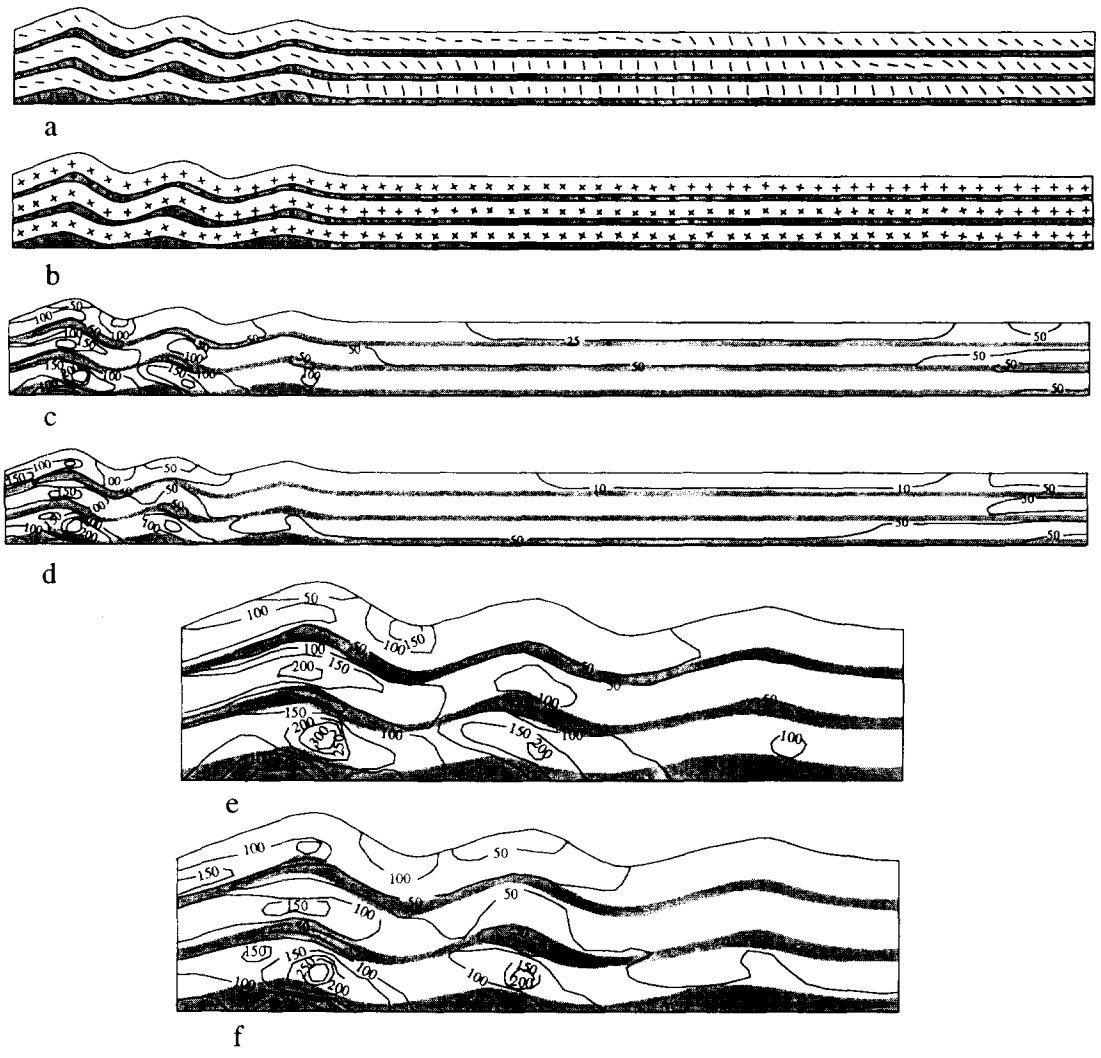

Fig. 7. Results of finite-element calculation for model F1. Boundary conditions as in Fig. 5. Horizontal compression is applied to the left-hand boundary. (a) Orientations of maximum principal stress (σ_1). (b) Orientations of the two planes of maximum shear stress (45° to σ_1). (c) Contour map showing the spatial variation of maximum principal stress (σ_1), MPa. (d) Contour map showing the spatial variation of differential stress ($\sigma_1 - \sigma_3$), MPa. For clarity the left-hand (hinterland) portions of (c) & (d) are reproduced at larger scale in (e) & (f).

Model with both folds and thrusts. From the analog modelling we observed that when the folds in the competent units had grown to a significant amplitude, faults propagated through the foreland-dipping fold limbs (see above and Fig. 3). Once present, thrust discontinuities in the strong units might be expected to influence the stress distribution within the fold stratigraphic pile. The next stage of the finite-element investigation was designed to assess this effect.

Model FT1 (Fig. 5c) represents a more advanced state of deformation than that of model F1, and is comparable to Stage III of the analog model (see Fig. 3). Two foreland-verging thrusts were incorporated into the foreland-dipping limbs of the first and second folds (counting from hinterland towards foreland) in the lowest strong unit. The first thrust cut completely through the layer and the second cut only through its lower half. In addition, a fourth anticlinal culmination was added to the fold train; there are thus two unfaulted folds in front of the folds that are cut by thrusts.

The spatial variation of the values of maximum principal stress (σ_1) and differential stress ($\sigma_1 - \sigma_3$) is shown by the contours in Figs. 8(a) & (b), respectively. Again for the sake of clarity, the left-hand (hinterland) portions of these plots are reproduced at enlarged scale in Figs. 8(c) & (d). The patterns are substantially similar to those in model F1 (Fig. 7), with stress concentrations in the foreland-dipping limbs of stiff-layer anticlines, especially in the lowest stiff layer. The discontinuities that were built into the lowest stiff layer have a significant effect; indeed, the differential stress reaches a value of over 300 MPa (the highest value in the model) at the tip of the right-hand discontinuity which cuts only the lower part of the layer. This indicates that fracture is likely to continue its propagation upwards through the layer.

An even more significant result of this model is that there are stress concentrations associated with the third and fourth anticlines in the lowest stiff unit. The stress concentration in the foreland-dipping limb of the third anticline is very strong, having a value equal to that around the first (left) thrust. The stress concentration in the third fold is greatly increased compared with that in

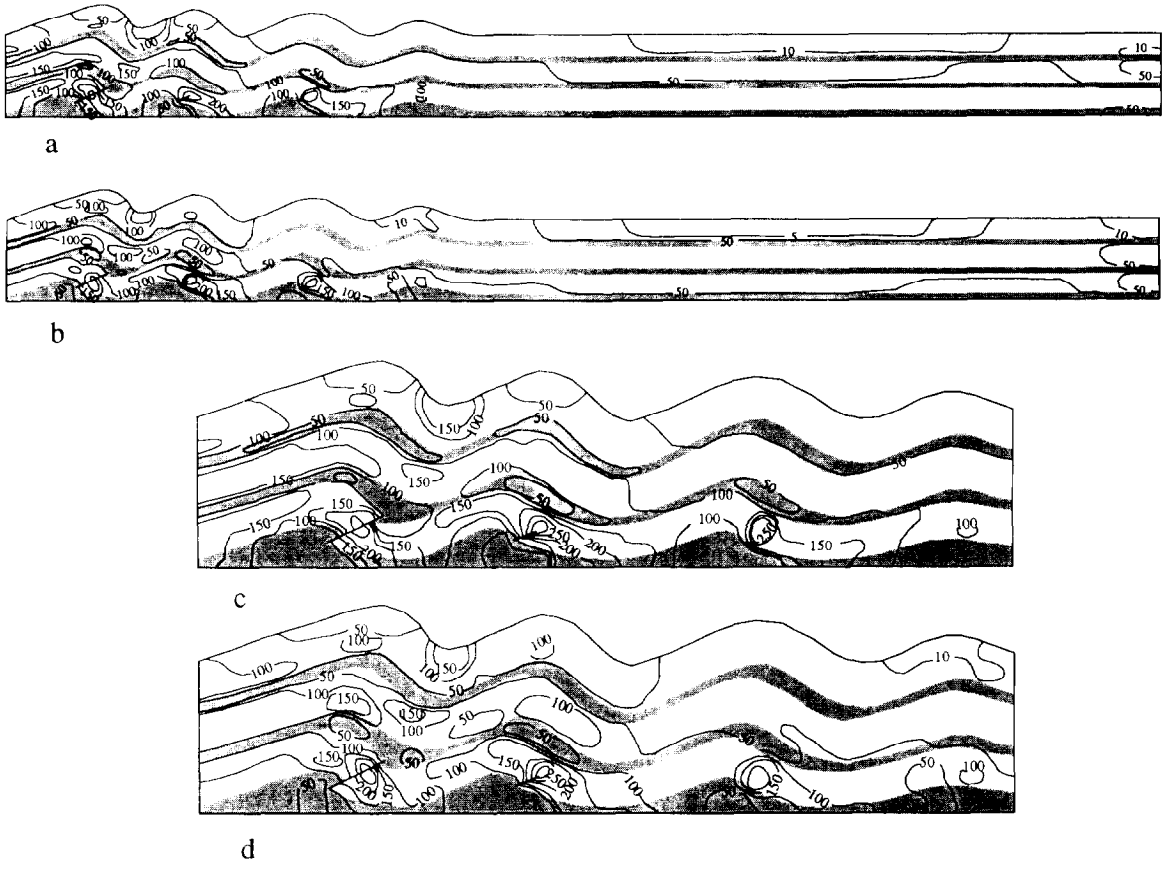

Fig. 8. Results of finite-element calculation for model FT1. Boundary conditions as in Fig. 5. Horizontal compression is applied to the left-hand boundary. (a) Contours showing the spatial variation of maximum principal stress (σ_1), MPa. (b) Contours showing the spatial variation of differential stress ($\sigma_1 - \sigma_3$), MPa. For clarity the left-hand (hinterland) portions of (a) & (b) are reproduced at larger scale in (c) & (d).

the equivalent fold in model F1 which has no thrusts (compare Figs. 8c & d with Figs. 7e & f). Model F1, with only three anticlines, exhibited a weak stress concentration associated with the limb of the right-most fold in the lowest stiff layer. Model FT1 has four anticlines, and again there is a weak stress concentration associated with the right-most one, notwithstanding the presence of the fracture discontinuities between the site and the hinterland boundary where the compressive load is applied. Therefore, the models demonstrate that as folds propagate towards the foreland, so do stress concentrations in their foreland-dipping limbs. Furthermore, thrust discontinuities have a weakening effect on the fold complex, and assist the foreland propagation of the stress concentrations.

DISCUSSION AND CONCLUSIONS

Our centrifuge models (of which Fig. 3 is just one typical example) demonstrate that thrust ramps can be localized by earlier-formed low-amplitude folds. Horizontal compression causes nucleation of folds in the foreland strata, with regular wavelength controlled by the rheological properties and relative thicknesses of the mechanical units (e.g. Biot 1961, 1964, Currie *et al.* 1962, Ramberg 1960, 1962, 1968, Smith 1969). Subsequently, thrust ramps nucleate serially from hinterland towards foreland, within the competent units, at sites which coincide with the foreland-dipping limbs of the folds.

Finite-element calculations on numerical models, with geometry and mechanical properties modelled on prototype systems also represented by the analog models, show that there are stress concentrations along the fore-limbs of the folds; the differential stress is much larger in these areas than anywhere else in the models. If the compressed wedge is going to fail, it will fail in these regions first. Furthermore, in models with cohesionless fractures within some of the folds, the stress concentrations persist and are associated with unfaulted folds further from the hinterland end of the model fold-thrust belt.

These relationships lead us to propose a generalized evolutionary model (Fig. 9) which explains the regularity of thrust spacing in natural duplex structures. Under horizontal compression the stratigraphic pile deforms by layer-parallel shortening and by buckle folding (Figs. 9a & b) (even if only of low amplitude). Stress concentrations (marked as dark areas in Fig. 9b) are associated with the foreland-dipping fold limbs. If the deforming mass subsequently undergoes brittle failure (Fig. 9c), this is most likely to initiate within the regions of stress concentration, that is, at sites localized by the folds. Furthermore, the orientation of the stress field within the areas of stress concentration favours propaga-

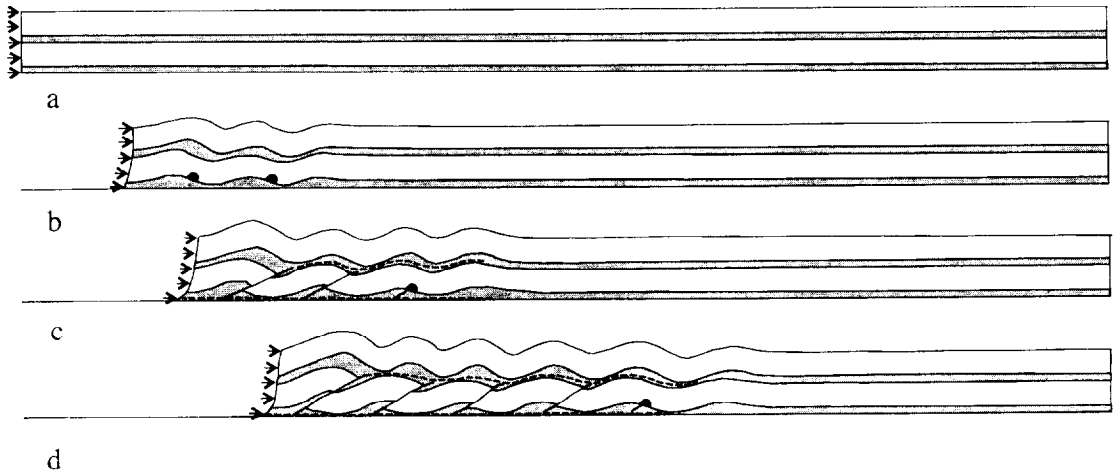

Fig. 9. Schematic illustration of formation of a duplex as a consequence of progressive buckling. Unornamented: competent units. Stippled: incompetent units. Dark regions in lower competent unit: sites of concentration of differential stress (and potential failure). Solid lines transecting lower competent unit: thrust ramps. Dashed lines within incompetent units: floor and roof thrusts of duplex structure. See text for detailed discussion.

tion of shear fractures at a low angle across the competent stratigraphic units, forming foreland-verging thrust faults, because of three factors: overall horizontal compression applied from the hinterland end, drag against the basement, and local rotation of the bedding to foreland-dipping attitude. The stress concentrations are greatest at the base of the lower competent stratigraphic units. The faults which ramp through these units are likely to merge with floor and roof thrusts within under- and overlying incompetent units, thus forming duplex structures (e.g. Morley 1994).

Continued horizontal compression of the deforming strata causes foreland propagation of the folding, which in turn causes further stress concentrations. Thus the processes of folding and thrust ramping propagate from hinterland towards foreland (Fig. 9d). However, the early-formed thrusts continue to accumulate displacement even while new ones are nucleating.

The stress concentration and brittle failure could occur at early, perhaps even incipient, stages of folding. In such cases, the deformation associated with fault drag and fault-bend folding would likely overprint and obscure any evidence of precursory buckling. Thus, the lack of clear evidence of earlier folding does not rule out the operation of this mechanism of ramp localization. Additional finite-element modelling is needed to assess the minimum fold amplitude required to generate a stress concentration that would cause faulting.

This model is consistent with the observation that fold wavelength and duplex ramp spacing are both linearly dependent on some measure of the thickness of strata involved in the two processes. Further investigation, applying theoretical models of fold mechanics to the actual multilayered sequences [e.g. along the line pursued by Goff *et al.* (1990)], is needed to determine whether there can be defined a suitable measure of 'effective thickness' (cf. Pollard & Johnson 1973) of strata, which resolves the discrepancy between the spacing of thrusts in natural duplex structures and the dominant wavelength of buckling in natural fold trains (Fig. 1).

On the basis of this relationship, it may be possible to predict the spacing of thrusts in a duplex structure through detailed investigation of the expected buckling wavelength of the specific stratigraphic succession involved. These results are relevant to petroleum exploration in fold-thrust belts, in so far as structural traps are associated with duplex ramps. This approach will likely be most useful in cases where the duplex is blind and situated at depth, such that other means of locating the ramps are unreliable or unavailable.

Acknowledgements—This work is based on Ph.D. research of S. Liu, who received a McLaughlin Fellowship and tuition bursary from Queen's University. Professor P. N. Gaskin of the Department of Civil Engineering, Queen's University, provided access to the ABAQUS software, and Dr H. Kong familiarized SL with the program. Computing facilities were provided by Queen's Department of Computing and Communications Services. The Experimental Tectonics Laboratory was constructed and is operated through grants from the Natural Sciences and Engineering Research Council of Canada to J. M. Dixon. Our modelling of fold-thrust tectonics has received support from ARCO Oil and Gas Co. The Geology Department of Otago University (New Zealand) kindly provided a congenial atmosphere for JMD's sabbatical during which his work on this manuscript was carried out. Geoff Rait provided helpful comments. The manuscript has been significantly improved after reviews by Dave Wiltschko, E. G. Bombalakis and Sue Treagus for which we are very grateful.

REFERENCES

Banks, C. J. & Warburton, J. 1986. "Passive-roof" duplex geometry in the frontal structures of the Kirthar and Sulaiman mountain belt, Pakistan. *J. Struct. Geol.* **8**, 229–237.

Berner, H., Ramberg, H. & Stephansson, O. 1972. Diapirism in theory and experiment. *Tectonophysics* **15**, 197–218.

Biot, M. A. 1961. Theory of folding of stratified viscoelastic medium and its application in tectonics and orogenesis. *Bull. geol. Soc. Am.* **72**, 1595–1520.

Biot, M. A. 1964. Theory of internal buckling of a confined multilayered structure. *Bull. geol. Soc. Am.* **75**, 563–568.

Bombalakis, E. G. 1986. Thrust-fault mechanics and origin of frontal ramps. *J. Struct. Geol.* **8**, 281–290.

Bombalakis, E. G. 1989. Thrust fault mechanics and dynamics during a developmental stage of a foreland belt. *J. Struct. Geol.* **11**, 439–455.

Boyer, S. 1991. Geometric evidence for synchronous thrusting in southern Alberta and northwest Montana thrust belts. In: *Thrust Tectonics* (edited by McClay, K.). Chapman & Hall, London, 377–390.

Boyer, S. & Elliott, D. 1982. Thrust systems. *Bull. Am. Ass. Petrol. Geol.* **66**, 1190–1230.
Burnett, D. S. 1987. *Finite Element Analysis: from Concepts to Applications*. Addison-Wesley, Reading, Massachusetts.
Carmichael, R. S. 1982. *Handbook of Physical Properties of Rocks*. CRC Press, Boca Raton, Florida, **3**.
Cello, G. & Nur, A. 1988. Emplacement of foreland thrust systems. *Tectonics* **7**, 261–271.
Chapple, W. M. 1978. Mechanics of thin-skinned fold-and-thrust belts. *Bull. geol. Soc. Am.* **89**, 1189–1198.
Currie, J. B., Patnode, H. W. & Trump, R. P. 1962. Development of folds in sedimentary strata. *Bull. geol. Soc. Am.* **73**, 655–674.
Dahlstrom, C. D. A. 1969. Balanced cross-sections. *Can. J. Earth Sci.* **6**, 743–757.
Dahlstrom, C. D. A. 1970. Structural geology in the eastern margin of the Canadian Rocky Mountains. *Bull. Can. Petrol. Geol.* **18**, 332–406.
Davis, D., Suppe, J. & Dahlen, F. A. 1983. Mechanics of fold-and-thrust belts and accretionary wedges. *J. geophys. Res.* **88**, 1153–1172.
De Bremacker, J. C. & Becker, E. B. 1978. Finite element models of folding. *Tectonophysics* **50**, 349–368.
Dieterich, J. H. 1969. Computer experiments on mechanics of finite amplitude folds. *Can. J. Earth Sci.* **7**, 467–476.
Dieterich, J. H. & Carter, N. E. 1969. Stress history of folding. *Am. J. Sci.* **267**, 129–154.
Dixon, J. M. & Liu, S. 1991. Centrifuge modelling of the propagation of thrust faults. In: *Thrust Tectonics* (edited by McClay, K.). Chapman & Hall, London, 53–70.
Dixon, J. M. & Summers, J. M. 1985. Recent developments in centrifuge modelling of tectonic processes: equipment, model construction techniques and rheology of model materials. *J. Struct. Geol.* **7**, 83–102.
Dixon, J. M. & Tirrul, R. 1991. Centrifuge modelling of fold-thrust structures in a tripartite stratigraphic succession. *J. Struct. Geol* **13**, 3–20.
Eisenstadt, G. & De Paor, D. G. 1987. Alternative model of thrust-fault propagation. *Geology* **15**, 630–633.
Elliott, D. & Johnson, M. R. W. 1980. The structural evolution of the northern part of the Moine thrust zone. *Trans. R. Soc. Edin.: Earth Sci.* **71**, 69–96.
Evans, M. A. 1989. The structural geometry and evolution of foreland thrust system, northern Virginia. *Bull. geol. Soc. Am.* **101**, 339–354.
Fermor, P. R. & Price, R. A. 1987. Multiduplex structure along the base of the Lewis thrust sheet in the southern Canadian Rockies. *Bull. Can. Petrol. Geol.* **35**, 159–185.
Goff, D. & Wiltschko, D. V. 1992. Stresses beneath a ramping thrust sheet. *J. Struct. Geol.* **14**, 437–449.
Goff, D., Wiltschko, D. V. & Fletcher, R. C. 1990. Folding as a controlling influence on the location of fault ramps within thrust belts. *Geol. Soc. Am. Abs. w. Prog.* **22**, A272.
Hafner, W. 1951. Stress distribution and faulting. *Bull. geol. Soc. Am.* **62**, 373–391.
Heim, A. 1878. *Untersuchungen über den Mechanismus der Gebirgsbildung*. Schwabe, Basel.
Hill, K. 1991. Structure of the Papuan fold belt, Papua New Guinea. *Bull. Am. Ass. Petrol. Geol.* **75**, 857–872.
Holl, J. E. & Anastasio, D. J. 1993. Structural partitioning of the Tertiary south Pyrenean foreland basin, Spain. *Geol. Soc. Am. Abs. w. Prog.* **25**, A167.
Jaeger, J. C. & Cook, N. G. W. 1979. *Fundamental of Rock Mechanics* (3rd edition). Chapman & Hall, London.
Jamison, W. R. 1987. Geometric analysis of fold development in overthrust terrains. *J. Struct. Geol.* **9**, 207–241.
Johnson, A. M. 1977. *Styles of Folding*. Elsevier, Amsterdam.
Liu, S. 1990. Centrifuge and numerical modelling of duplex structures. Ph.D. Thesis, Queen's University.
Liu, S. & Dixon, J. M. 1990. Centrifuge modelling of thrust faulting: strain partitioning and the sequence of thrusting in duplex structures. In: *Deformation Mechanisms, Rheology and Tectonics* (edited by Knipe, R. J.). *Spec. Publ. geol. Soc. Lond.* **54**, 431–444.
Liu, S. & Dixon, J. M. 1991. Centrifuge modelling of thrust faulting: structural variation along strike in fold-thrust belts. *Tectonophysics* **188**, 39–62.
Mandl, G. & Shippam, G. K. 1981. Mechanical model of thrust sheet gliding and imbrication. In: *Thrust and Nappe Tectonics* (edited by McClay, K. R. & Price, N. J.). *Spec. Publ. geol. Soc. Lond.* **9**, 79–98.
McMechan, M. E. 1985. Low-taper triangle-zone geometry: an interpretation of the Rock Mountain Foothills, Pine Pass–Peace River area, British Columbia. *Bull. Can. Petrol. Geol.* **33**, 31–38.
Mitra, S. 1986. Duplex structures and imbricate thrust systems: geometry, structural position, and hydrocarbon potential. *Bull. Am. Ass. Petrol. Geol.* **70**, 1087–1112.
Mitra, S. & Namson, J. 1989. Equal-area balancing. *Am. J. Sci.* **289**, 563–599.
Morley, C. K. 1994. Fold-generated imbricates: examples from the Caledonides of Southern Norway. *J. Struct. Geol.* **16**, 619–631.
Müller, W. H. & Briegel, B. U. 1980. Mechanical aspects of the Jura overthrust. *Eclog. geol. Helv.* **73**, 239–250.
Platt, J. P. 1988. The mechanics of frontal imbrication: a first-order analysis. *Geol. Rdsch.* **77**, 577–589.
Pollard, D. D. & Johnson, A. M. 1973. Mechanics of growth of some laccolithic intrusions in the Henry Mountains, Utah, II. *Tectonophysics* **18**, 311–354.
Price, R. A. 1981. The Cordilleran foreland thrust and fold belt in the southern Canadian Rocky Mountains. In: *Thrust and Nappe Tectonics* (edited by McClay, K. R. & Price, N. J.). *Spec. Publ. geol. Soc. Lond.* **9**, 427–448.
Protzman, G. M. & Mitra, G. 1990. Strain fabric associated with the Meade thrust sheet: implications for cross-section balancing. *J. Struct. Geol.* **12**, 403–417.
Ramberg, H. 1960. Relationship between arc length and thickness of ptygmatically folded veins. *Am. J. Sci.* **258**, 36–46.
Ramberg, H. 1962. Contact strain and folding instability of a multilayered body under compression. *Geol. Rdsch.* **51**, 405–439.
Ramberg, H. 1967. *Gravity, Deformation and the Earth's Crust as Studied by Centrifuge Models*. Academic Press, London.
Ramberg, H. 1968. Instability of layered systems in the field of gravity. *Phys. Earth & Planet. Interiors* **1**, 427–447.
Ramberg, H. 1981. *Gravity, Deformation and the Earth's Crust in Theory, Experiments and Geological Applications* (2nd edition). Academic Press, London.
Reddy, J. N. 1984. *An Introduction to the Finite Element Method*. McGraw-Hill, New York.
Schedl, A. & Wiltschko, D. V. 1987. Possible effects of pre-existing basement topography on thrust fault ramping. *J. Struct. Geol.* **9**, 1029–1037.
Schirmer, T. W. 1988. Structural analysis using thrust-fault hanging-wall sequence diagrams: Ogden duplex, Wasatch Range, Utah. *Bull. Am. Ass. Petrol. Geol.* **72**, 573–585.
Skuce, A. G., Gordy, N. P. & Maloney, J. 1992. Passive-roof duplexes under the Rocky Mountain Foreland Basin, Alberta. *Bull. Am. Ass. Petrol. Geol.* **76**, 67–80.
Smith, R. B. 1969. The folding of a strongly non-Newtonian layer. *Am. J. Sci.* **279**, 272–287.
Suppe, J. 1983. Geometry and kinematics of fault-bend folding. *Am. J. Sci.* **283**, 684–721.
Suppe, J. 1985. *Principles of Structural Geology*. Prentice-Hall, Englewood Cliffs, New Jersey.
Suppe, J. & Medwedeff, D. A. 1984. Fault-propagation folding. *Geol. Soc. Am. Abs. w. Prog.* **16**, 670.
Suppe, J. & Medwedeff, D. A. 1990. Geometry and kinematics of fault-propagation folding. *Eclog. geol. Helv.* **83**, 409–454.
Tirrul, R. 1983. Structure cross-sections across Asiak Foreland Thrust and Fold Belt, Wopmay Orogen, District of Mackenzie. *Geol. Surv. Can. Pap.* **84-1B**, 253–260.
Touloukian, Y. S., Juddy, W. R. & Roy, R. D. 1981. *Physical Properties of Rocks and Minerals*. McGraw-Hill, New York.
Townsend, C., Roberts, D., Rice, A. H. N. & Gayer, R. A. 1986. The Gaissa Nappe, Finnmark, North Norway: an example of deeply eroded external imbricate zone within the Scandinavian Caledonides. *J. Struct. Geol.* **8**, 431–440.
Treagus, S. H. 1981. A theory of stress and strain variation in viscous layers, and its geological implications. *Tectonophysics* **72**, 75–103.
Treagus, S. H. 1983. A theory of finite strain variation through contrasting layers, and its bearing on cleavage refraction. *J. Struct. Geol.* **5**, 351–368.
Willis, B. 1893. The mechanics of Appalachian structure. *Ann. Rep. U.S. Geol. Surv.* **13**, Part II, 211–282.
Wiltschko, D. V. & Eastman, D. B. 1983. Role of basement warps and faults in localizing thrust fault ramps. *Mem. geol. Soc. Am.* **158**, 177–190.
Wiltschko, D. V. & Eastman, D. B. 1988. A photoelastic study of the effects of pre-existing reverse faults in basement on the subsequent deformation of the cover. In: *Interaction of the Rocky Mountain Foreland and the Cordilleran Thrust Belt* (edited by Schmidt, C. J. & Perry, W. J.). *Mem. geol. Soc. Am.* **171**, 111–118.
Woodward, N. B. 1985. Valley and Ridge thrust belt: balanced structural sections, Pennsylvania to Alabama. *Appalachian Basin Industrial Associates Studies in Geology* **12**, University of Tennessee.